Short communication

# Preparation of Pt supported on WO₃–C with enhanced catalytic activity by microwave-pyrolysis method

Jilei Ye[a], Jianguo Liu[a,b,*], Zhigang Zou[a,b,**], Jun Gu[a], Tao Yu[a]

[a] *Eco-materials and Renewable Energy Research Center, Department of Physics and National Laboratory of Solid State Microstructures, Nanjing University, Nanjing 210093, China*
[b] *Department of Materials Science and Engineering, Nanjing University, Nanjing 210093, China*

## ARTICLE INFO

## ABSTRACT

The WO₃–C hybrid materials are prepared by intermittently microwave-pyrolysis using ammonium tungstate as the precursor, and then Pt nano-particles are deposited by microwave-assited polyol process on WO₃–C. The TEM images show the dispersion of ∼10 nm WO₃ particles size supported on carbon and ∼3 nm Pt metal crystallites supported on WO₃–C. XRD results illustrate that WO₃ presented as monoclinic phase and the content of WO₃ in WO₃/C and Pt/WO₃–C catalysts is further characterized by EDAX. Furthermore, XPS characterizations indicate that the interaction between Pt and WO₃ is dramatically enhanced after heat treatment at 200 °C. The activities of Pt/WO₃–C for the electrochemical oxidation of methanol are compared with Pt/C in acid solution by cyclic voltammetry, CO-stripping and chronoapperometry. Pt/WO₃–C catalyst calcined at 200 °C exhibits the highest activity per electrochemical active surface area for methanol oxidation and is 60 mV more negative for CO electro-oxidation than that of Pt/C and Pt/WO₃–C without heat treatment. The great enhancement of electrochemical performance may be due to the improvement of the synergistic effect between Pt and WO₃ in Pt/WO₃–C catalyst after heat treatment.

## 1. Introduction

The anode catalysts of direct methanol fuel cell (DMFC) have been explored to solve the low kinetic process of methanol electro-oxidation and CO-poisoned problems for several decades. It is demonstrated that there are great improvements in terms of promotion effect or bi-functional effect when Pt was modified by other metals or metal oxides. The well-known electrocatalysts of Pt–Ru [1–3], Pt–Ru–Os [4], Pt–Ru–W [5], Pt–Ru–Ir [6,7] and Pt–Ru–Sn [8] perform significantly better than Pt alone. Various factors including particle-size, composition, and electronic structure of Pt after modification and structural arrangements in the nanostructure have also been reported. Besides, some studies claimed that the addition of metal oxides (TiO₂ [9], ZrO₂ [10], MoO₃ [11], CeO₂ [12,13], SnO₂ [14], etc.) effectively promote the electro-oxidation of methanol, which is due to the high dispersion of Pt nano-particles, the stabilization of Pt on support and the

formation of OH species under lower potential with the additive promoter. Especially, Pt/WO₃–C electrocatalysts prepared by various synthesis procedures [15–19] are known to greatly enhance the electro-oxidation of methanol. The H-spillover effect from Pt to WO₃ left more free Pt active sites to accelerate kinetics of methanol dehydrogenation [20,21]; meanwhile, the H$_x$WO₃ is a good conductor, unlike most metal oxides of low conductivity. However, the morphology of WO₃ and the interaction between Pt and WO₃ are still in vague [21,22], which are two key parameters to improve the electro-oxidation of methanol and CO.

In this study, Pt/WO₃–C was prepared by a new method, i.e. WO₃–C hybrid materials were firstly synthesized by intermittently microwave-pyrolysis, and then Pt particles were deposited on it. The results indicated that WO₃ with small particles was well dispersed on carbon, and the catalytic performance of Pt/WO₃–C was improved further after heat treatment at 200 °C. The relationship between the structure of Pt/WO₃–C and performance of methanol oxidation was discussed as well.

## 2. Experimental

### 2.1. Sample preparation

Ammonium tungstate was mixed mechanically with carbon (Vulcan XC-72, Cobat Corp.) for 30 min using ethanol as solvent. The

* Corresponding author at: Department of Materials Science and Engineering, Nanjing University, 22 Hankou Road, Nanjing 210093, China. Tel.: +86 25 83621219; fax: +86 25 83686632.
** Corresponding author at: Department of Physics, Nanjing University, 22 Hankou Road, Nanjing 210093, China. Tel.: +86 25 83686632.
*E-mail addresses:* jianguoliu@nju.edu.cn (J. Liu), zgzou@nju.edu.cn (Z. Zou).

paste was dried under 60 °C for 20 h and then ground for later usage. The powder was placed in the center of a household microwave oven (2450 MHz, 700 W) and intermittently heated in the form of pulse every 10 s for three times. The hybrid material was denoted as $WO_3$–C, in which the theoretical weight ratio of $WO_3$ to C is 10:90.

Microwave-assisted glycol method was chosen to load Pt on C or $WO_3$–C support in ethylene glycol solution with $H_2PtCl_6$ as precursor [23]. Moreover, Pt/$WO_3$–C catalyst was calcined at 200 °C in $N_2$ atmosphere for 2 h, which was denoted as Pt/$WO_3$–C–HT. Pt loading was kept as 10 wt% in all samples.

### 2.2. Physical and electrochemical characterizations

The particle-size distribution and morphology of catalysts were examined by transmission electron microscope (TEM) on a FEI Tecnai20 FEG at 200 kV. The distribution of elemental concentrations was performed using the mapping analysis of SEM (LEO 1530VP) equipped with energy dispersive analysis of X-ray spectrometer (EDAX).

X-ray diffraction (XRD) measurements were carried out with a Rigaku D/MAX-Ultima III X-ray diffractometer using Cu Kα radiation ($\lambda$ = 0.15406 nm). The $2\theta$ angular ranges between 20° and 80° were explored at a scan rate of 10° $min^{-1}$. The X-ray photoelectron spectroscopy (XPS) measurement was performed by ESCALAB 250 apparatus, using monochromated Al Kα radiation at 150 W, in the pass energy (PE) mode (PE = 20 eV). All of the spectra were obtained under identical conditions. The pressure of the spectrometer was $5 \times 10^{-10}$ mbar and $5 \times 10^{-9}$ mbar during the measurements.

Electrochemical experiments were conducted by an electrochemical workstation (PARSTAT 2273, Princeton Applied Research) equipped with a three-electrode configuration using Pt foil as a counter electrode, and saturated calomel electrode (SCE) as a reference. The working electrodes were fabricated by casting Nafion-impregnated catalyst ink onto 0.196 $cm^2$ glass carbon disk electrodes, and the loading of the catalyst was 0.255 mg $cm^{-2}$. For CV measurements, the working electrode was immersed in nitrogen saturated 0.5 M $CH_3OH$ in 0.5 M $H_2SO_4$ solution. In the CO-stripping experiment, the pre-adsorption of CO was achieved by bubbling CO gas into the solution, while the potential of working electrode was kept at −0.15 V versus SCE for 20 min. After that, the solution was purged with $N_2$ gas for another 20 min to remove the dissolved CO in the solution.

In electro-catalytic investigations, electrochemical active surface area (ECSA) of each electrode was used to normalize the current density. ECSA of the Pt-based working electrodes were determined from CO-stripping voltammograms.

## 3. Results and discussion

### 3.1. XRD characterization

The XRD patterns of Pt/C and Pt/$WO_3$–C catalysts were shown in Fig. 1. The diffraction peaks at 39.6°, 46.3° and 67.4° observed in samples corresponding to the face-centered cubic (fcc) phase of Pt [24], while those at 33°, 40°, 49°, 54°, 61° and 76° observed in Pt/$WO_3$–C catalysts corresponding to the monoclinic phase of $WO_3$ [25,26]. The diffraction peaks at 23° in all catalysts were due to the mixture of the (0 0 2) reflection of Vulcan XC-72 carbon and (0 2 0) reflection of $WO_3$. In all samples, the diffraction peak intensity of Pt (2 2 0) at 67.4° was too weak to calculate the Pt crystallize size. However, each diffraction peak of Pt crystalline plane was obviously broad, meaning Pt nano-particles were small in these catalysts.

It was clear that $WO_3$ particles with high crystalline monoclinic phase presented in $WO_3$–C hybrid material as shown in Fig. 1(b) and (c). No other new phases were observed after heat treatment at 200 °C. As reported in literature, the addition of
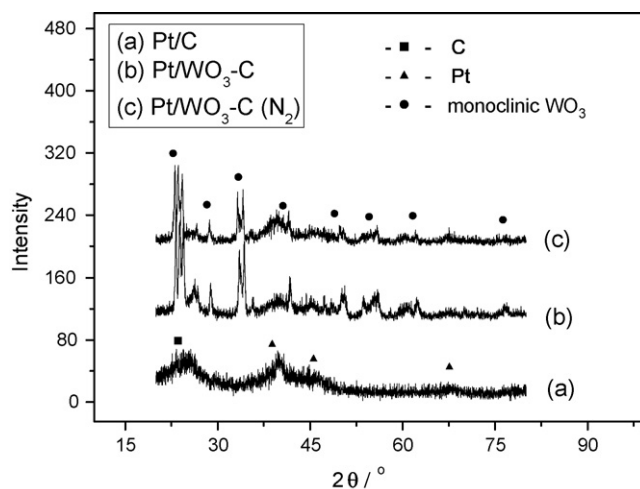


**Fig. 1.** XRD patterns of (a) Pt/C, (b) Pt/$WO_3$–C and (c) Pt/$WO_3$–C–HT samples.

$WO_3$ in Pt/C by various methods [27,28] can enhance the activity for methanol electro-oxidation due to the formation of hydrogen tungsten bronze. However, the size of $WO_3$ particles is hardly controlled, which is believed to be important to maximize interfaces of Pt/$WO_3$. By microwave-pyrolysis method proposed in this paper, $WO_3$ crystalline formed quickly due to unique microwave-absorption property of carbon material, which can intermediately decompose tungstate precursor to form $WO_3$–C hybrid material and avoid the following aggregation of $WO_3$ particles, which happens in the conventional pyrolysis or hydrolysis method.

### 3.2. TEM characterization

Fig. 2 presented the TEM of Pt/C, $WO_3$–C, Pt/$WO_3$–C and Pt/$WO_3$–C–HT samples. As shown in Fig. 2(a), around 3 nm Pt nano-particles were homogenously dispersed on carbon in Pt/C catalysts. It was seen from Fig. 2(b) that 6–15 nm $WO_3$ nano-particles were deposited on carbon. The crystalline plane distance was 0.382 nm, which was in agreement with (0 1 0) of monoclinic phase $WO_3$ as shown in Fig. 2 (pdf#30-1387). The formation of relatively small $WO_3$ particles tended to be helpful for separating Pt nano-particles and maximizing the interfaces of Pt/$WO_3$. The Fig. 2(c) gave the TEM results of Pt supporting on $WO_3$–C hybrid material. Although the microstructure of Pt and $WO_3$ was hardly to be distinguished, the uniform dispersion of small Pt or $WO_3$ particles on carbon support was clear. Comparing between Fig. 2(c) and (d), the particles size showed no obvious change after heat treatment in $N_2$ atmosphere. It was interesting to notice that particle-size and shape were changed when $WO_3$ existed in Pt/C. It may be due to the co-existence of Pt and $WO_3$ particles on carbon support. Therefore, the abundant interfaces between Pt and $WO_3$ were likely to generate, which can enhance the H-spill effect and improve the catalytic activity.

The chemical composition of the obtained $WO_3$–C, Pt/$WO_3$–C and Pt/$WO_3$–C–HT samples was determined by EDAX analysis. Table 1 listed the content of each composite for all samples. The

**Table 1**
EDAX analysis of all samples.

| Samples | Element (wt%) | | | |
|---|---|---|---|---|
| | C | W | Pt | O |
| $WO_3$–C | 84.75 | 9.11 | – | 6.14 |
| Pt/$WO_3$–C | 74.65 | 9.03 | 9.46 | 6.86 |
| Pt/$WO_3$–C–HT | 72.28 | 9.28 | 9.81 | 8.63 |
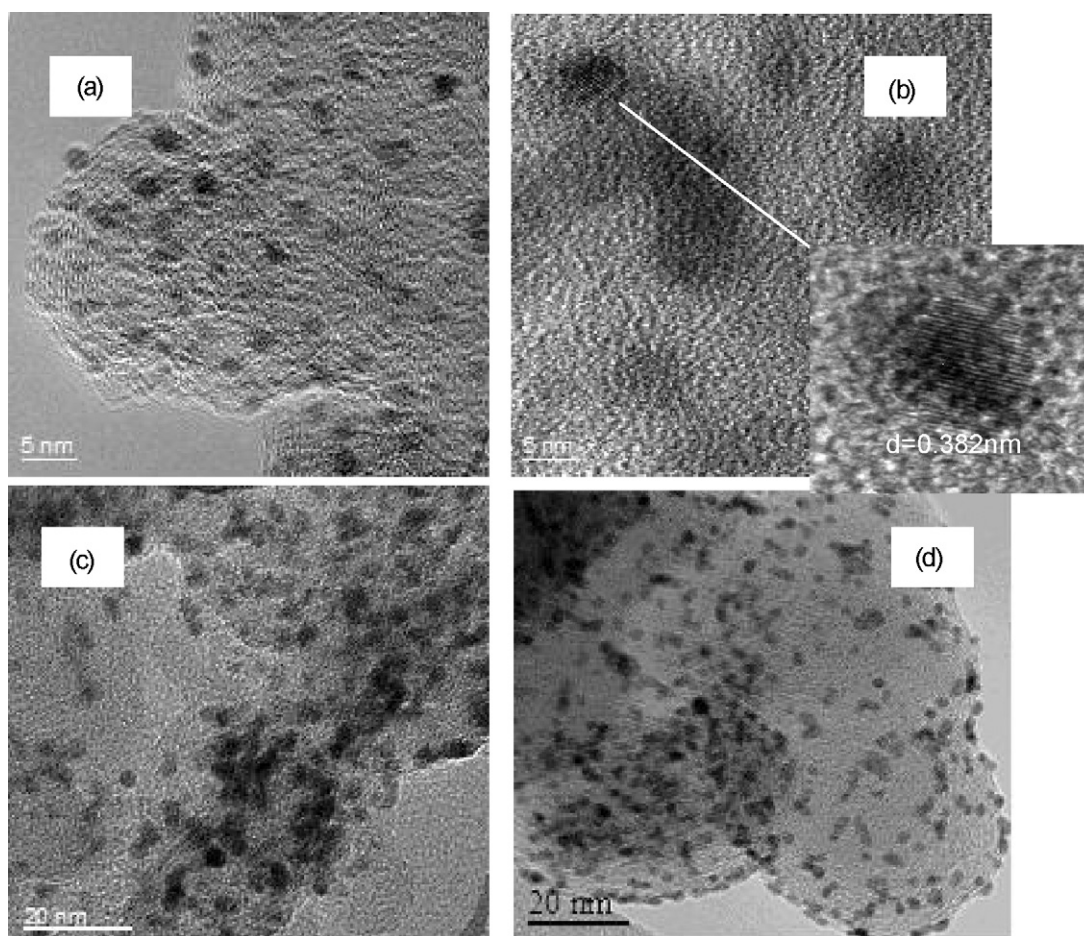
**Fig. 2.** TEM images of (a) Pt/C, (b) $WO_3$/C, (c) Pt/$WO_3$–C and (d) Pt/$WO_3$–C–HT samples.

element composition and contents were taken in different particular microzones. From the EDAX spectrum, the existence of the $WO_3$ in all samples was testified. The contents of W in $WO_3$/C, Pt/$WO_3$–C and Pt/$WO_3$–C–HT were 9.11%, 9.03% and 9.28%, separately, which were close to the initial ratio of 10 wt%. It cannot be excluded that a small quantity of tungstate decomposed incompletely, but there was little change of W content in three samples. A slight increase of the ratio of Pt:W in Pt/$WO_3$–C–HT may be due to the aggregation of Pt nano-particles. Based on the results of TEM and EDAX, $WO_3$ with nano-particles can be deposited successfully by intermittently microwave-pyrolysis method.

### 3.3. XPS analysis

Fig. 3 exhibited the XPS results of Pt 4f and W 4f. The binding energies (BE) of all peaks were referenced to a C1s value of 284.6 eV. All samples demonstrated similarly asymmetric peaks, indicating multiple oxidation states for Pt. The principle peaks were assigned to $Pt^0$ at 71.4 eV ($4f_{7/2}$) and 74.7 eV ($4f_{5/2}$), where double shoulder peaks at 73.0 eV and 75.8 eV were due to PtO or Pt(OH)$_2$ [29]. For all samples, platinum mostly existed in the form of metal Pt, containing little $Pt^{2+}$. It can be seen that the Pt 4f peaks nearly unchanged in Pt/$WO_3$–C without heat treatment. The W 4f spectrum of Pt/$WO_3$–C was also exhibited in Fig. 3. The two major peaks at 36.1 eV and 38.1 eV were assigned to the +6 oxidation state of tungsten for the W $4f_{7/2}$ and W $4f_{5/2}$ [30], respectively. It was clear that the tungsten majorly exists in a +6 valence state, but there was also a small fraction of $W^{5+}$, centering at 35.0 eV and 36.8 eV [30]. Noticeably, the binding energy of Pt 4f and W 4f peaks shifted after calcination, probably due to various electronic interactions between Pt and

support. The phenomenon was a symbol of strong "metal–support interaction" between Pt and $WO_3$. This kind of interaction can modify the electronic and catalytic properties of metal nano-particles and lead to the electrochemical activation of both dispersed metal and oxide. Recently, Pd/$WO_3$–C was reported for oxygen reduction reaction and the researchers found that the uniform dispersion of Pd on $WO_3$/C and the strong interaction between Pd and $WO_3$ from XPS greatly improve the catalytic performance [31].

As we know, it was hard to use sol–gel method to disperse noble metal particles on hydrophobic supports in acid solution, such as $WO_3$ with a low isolectric point of 0.43 [32]. In this work, there was no change of Pt 4f XPS comparing between Pt/C and fresh Pt/$WO_3$–C catalysts, indicating the interaction between Pt and $WO_3$ was quite weak by sol–gel method. After heat treatment, the interaction between Pt and $WO_3$ was dramatically improved and more interfaces of Pt/$WO_3$ may emerge.

### 3.4. CO-stripping voltammograms and methanol electro-oxidation activity

For Pt/$WO_3$–C catalyst, it was hard to calculate the Pt surface area obtaining from H-UPD measurements, which was due to the intercalation of protons in $WO_3$ forming tungsten bronzes, which occurs in the same potential region (−0.24 to 0.05 vs SCE) as H-UPD on Pt [33]. Therefore, CO-stripping tests were investigated to calculate the electrochemical surface area (ECSA) in Fig. 4. Assuming CO monolayer adsorption charge of $Q^0 = 420\ \mu C\ cm^{-2}$, the ECSA was calculated by $Q/[Pt]Q^0$, where $Q$ was the charge transferred derived from the electro-oxidation of CO on the surface of platinum, and [Pt] represented the Pt loading in the electrode. According to
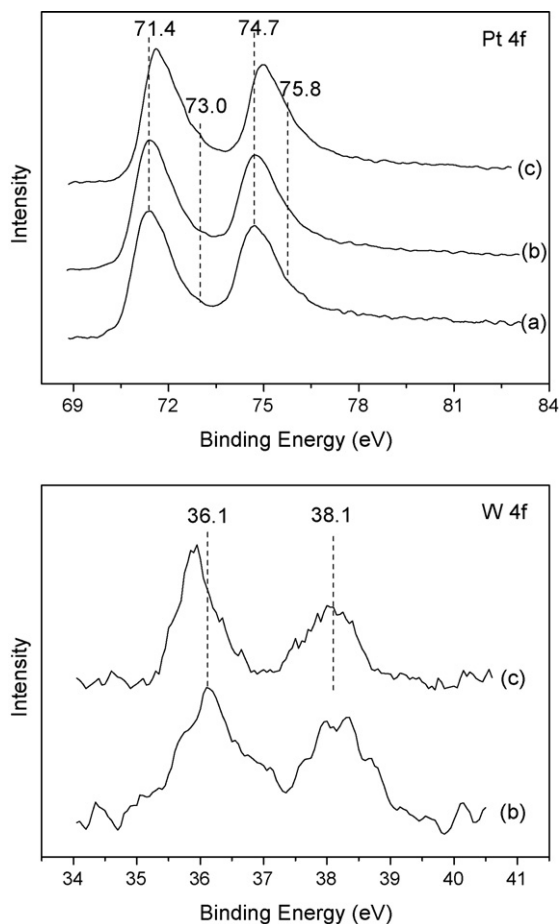
**Fig. 3.** Pt 4f, W 4f XPS spectra of (a) Pt/C, (b) Pt/WO$_3$–C and (c) Pt/WO$_3$–C–HT samples.

Fig. 4, the ECSA increased from 72.1 to 114.8 m$^2$ g$^{-1}$, while after heat treatment the ESA by calculation further increased to 133.1 m$^2$ g$^{-1}$. According to TEM, small particles WO$_3$ was loaded in carbon support by microwave decompose, in favor of the dispersion of Pt nano-particles on support and the enhancement of ECSA. After heat treatment, the electro-oxidation current of CO$_{ads}$ species further
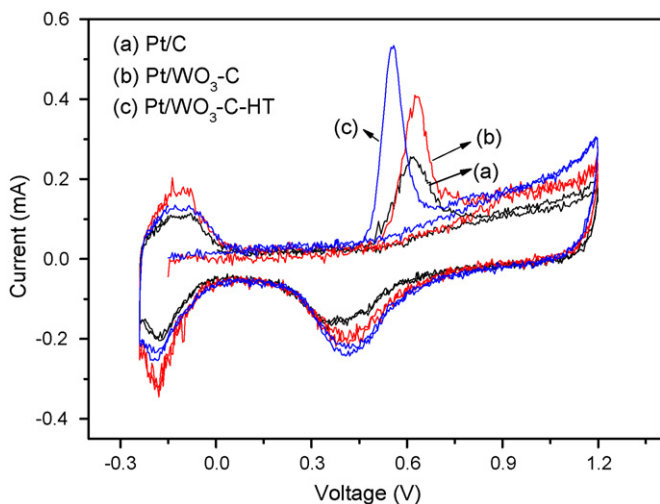


**Fig. 4.** CO-stripping voltammetry of saturated CO in 0.5 M H$_2$SO$_4$ solution for (a) Pt/C, (b) Pt/WO$_3$–C and (c) Pt/WO$_3$–C–HT catalysts. Scan rate = 20 mV s$^{-1}$ at room temperature.
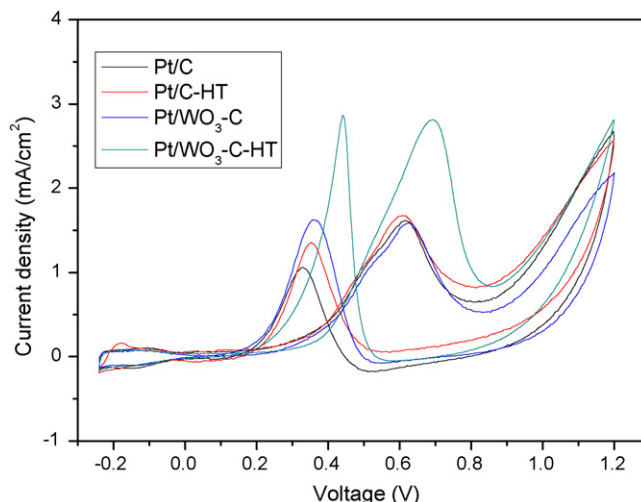


**Fig. 5.** Cyclic voltammograms for Pt/C and Pt/WO$_3$–C. Scan rate = 20 mV s$^{-1}$ at room temperature in 0.5 M H$_2$SO$_4$ with 0.5 M CH$_3$OH. (a) Pt/C, (b) Pt/WO$_3$–C and (c) Pt/WO$_3$–C–HT.

increased, which can be due to the maximized interaction between Pt and WO$_3$. It was reported by Hou [34] that the CO$_{ads}$ on Pt sites can spill on neighbor WO$_3$ particles adsorbing OH species. The rapid oxidation will form more free Pt sites covered by CO, resulting in the increase of CO electro-oxidation current.

In addition, the onset potential of CO electro-oxidation with Pt/WO$_3$–C–HT was 0.439 V, which was 60 mV negative than Pt/C and fresh Pt/WO$_3$–C. It was also proved that WO$_3$–C catalyst showed no activity for methanol and CO electro-oxidation (not shown in this work). That was to say, the WO$_3$ connected with active Pt sites, can promote CO oxidation dramatically. The interaction between Pt and WO$_3$ possibly modified the electron density of Pt sites and weakened the CO absorbing bond on Pt. Therefore, more sites of Pt interacting with WO$_3$ were helpful for improving the electro-oxidation ability of CO.

Fig. 5 depicted cyclic voltammogram of catalyst samples performed in a solution containing 0.5 M CH$_3$OH/0.5 M H$_2$SO$_4$. Although the peak current increased from 0.584 mA of Pt/C to 0.916 mA of Pt/WO$_3$–C (not shown in this work), the current density of methanol electro-oxidation on both Pt/C and Pt/WO$_3$–C catalysts was very close. Interestingly, Pt/WO$_3$–C–HT catalyst exhibited much higher peak current density of 2.84 mA cm$^{-2}$ than 1.62 mA cm$^{-2}$ of Pt/C catalyst, demonstrating an intrinsic enhancement of catalytic performance.

To clearly investigate the effect of the interaction between Pt and WO$_3$ on Pt/WO$_3$–C–HT catalyst performance, we also performed methanol electro-oxidation on Pt/C–HT catalysts, as seen in Fig. 5. It was obvious that the current density of methanol oxidation per ECSA was nearly unaffected by the heat treatment for Pt/C catalyst. So the strong interaction between Pt and WO$_3$ may be the dominant factor greatly promoting the catalytic performance. The abundant interfaces of Pt/WO$_3$ can improve H-spill effect, which can keep Pt sites clear for chemisorption of methanol, thus advance the kinetic of methanol dehydrogenation.

### 3.5. Chronoamperometric tests

To show the electrochemical stability of the three catalysts for methanol oxidation, chronoamperometric experiments were carried out. The current–time curves for the three catalysts in 0.5 M CH$_3$OH and 0.5 M H$_2$SO$_4$ at 0.4 V and 0.6 V versus SCE were shown in Fig. 6. All catalysts showed gradual decay in the current in test time, which may be due to the poison of CO intermediate species
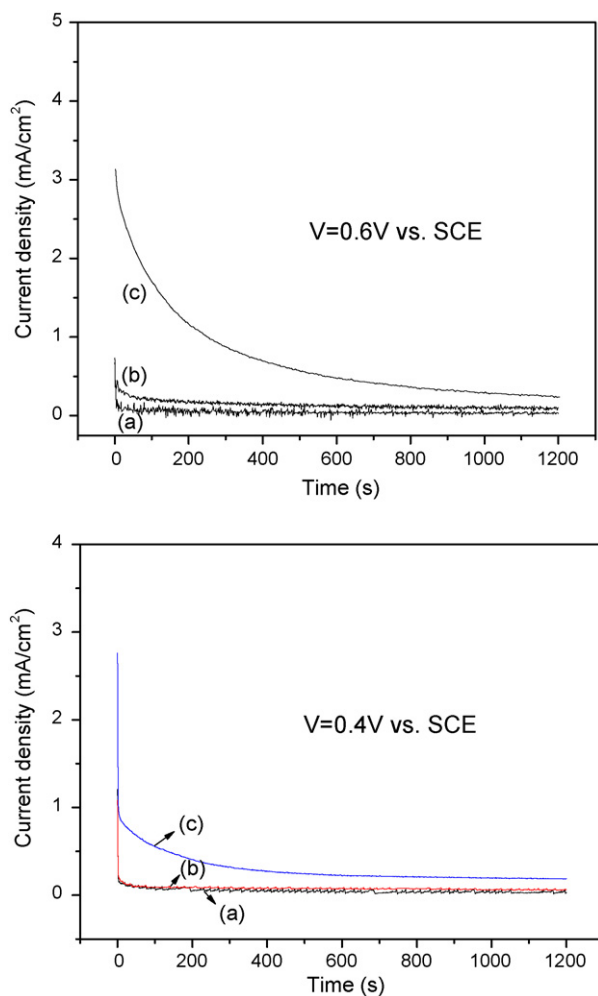
**Fig. 6.** Chronoamperometric curves for methanol eletro-oxidation on (a) Pt/C, (b) Pt/WO$_3$–C and (c) Pt/WO$_3$–C–HT catalysts in 0.5 M H$_2$SO$_4$ with 0.5 M CH$_3$OH under different potentials.

on active sites. Compared with Pt/C, Pt/WO$_3$–C catalyst showed a little higher activity than Pt/C catalyst at 0.6 V. For Pt/WO$_3$–C–HT catalyst, the current density per ECSA both at 0.6 V and 0.4 V dropped much less seriously than that of the other two catalysts, and showed the best electro-catalytic performance and kept higher than the other catalysts during 20 min. According to the CO-stripping voltammetry, the potential of CO electro-oxidation was lower on Pt/WO$_3$–C–HT, which may be helpful to keep more Pt active sites to methanol dehydrogenation and the decomposition of water molecular to form –OH species. The intrinsic catalytic activity on Pt/WO$_3$–C–HT enhanced obviously according to the increase of current density per ECSA, explaining that Pt sites of Pt/WO$_3$–C–HT were more active for methanol electro-oxidation. Above all, Pt/WO$_3$–C–HT catalyst gave the best performance and the best stability among three catalysts due to the high ECSA and the strong interaction between Pt and WO$_3$.

## 4. Conclusions

WO$_3$ particles with a size of ~10 nm were deposited on XC-72 carbon by microwave-pyrolysis method. EDAX results further revealed the existence of tungsten with certain weight ratio in WO$_3$/C and Pt/WO$_3$–C catalysts. Pt supported on WO$_3$–C showed higher activity for methanol electro-oxidation than that of Pt/C catalyst. The TEM and cyclic voltammetry results indicated that the addition of WO$_3$ in Pt/C catalyst was in favor of improving the distribution of Pt nano-particles and the electrochemical surface area. Furthermore, Pt/WO$_3$–C after heat treatment at 200 °C exhibited higher intrinsic activity for methanol and CO elctrooxidation. The H-spill effect due to strong interaction between Pt and WO$_3$ plays a critical role on methanol oxidation for Pt/WO$_3$–C catalyst.

## Acknowledgements

## References

[1] M. Watanabe, M. Vehida, S. Motoo, J. Electroanal. Chem. 229 (1987) 395–406.
[2] S. Wasmus, W. Vielstich, J. Appl. Electrochem. 23 (1993) 120–124.
[3] Z.L. Liu, X.Y. Ling, B. Guo, L. Hong, J.Y. Lee, J. Power Sources 167 (2007) 272–280.
[4] K.L. Ley, R. Liu, C. Pu, Q. Fan, N. Leyarovska, C. Segre, E.S. Smotkin, J. Electrochem. Soc. 144 (1997) 1543–1548.
[5] Z.B. Wang, P.J. Zuo, G.P. Yin, J. Alloys Compd. 479 (2009) 395–400.
[6] D.S. Geng, D. Matsuki, J.J. Wang, T. Kawaguchi, W. Sugimoto, Y. Takasu, J. Electrochem. Soc. 156 (2009) B397–B402.
[7] P. Sivakumar, V. Tricoli, Electrochem. Solid-State Lett. 9 (2006) A167–A170.
[8] T. Kim, M. Takahashi, M. Nagai, K. Kobayashi, Chem. Lett. 33 (2004) 478–479.
[9] H.Q. Song, X.P. Qiu, D.J. Guo, F.S. Li, J. Power Sources 178 (2008) 97–102.
[10] N.F.P. Ribeiro, F.M.T. Mendes, C.A.C. Perez, M.M.V.M. Souza, M. Schmal, Appl. Catal. A 347 (2008) 62–71.
[11] T. Ioroi, T. Akita, S. Yamazaki, Z. Siroma, N. Fujiwar, K. Yasuda, Electrochim. Acta 52 (2006) 491–498.
[12] M.A. Scibioh, S.K. Kim, E.A. Cho, T.H. Lim, S.A. Hong, H.Y. Ha, Appl. Catal. B 84 (2008) 773–782.
[13] J.S. Wang, J.Y. Xi, Y.X. Bai, Y. Shen, J. Sun, L.Q. Chen, W.T. Zhu, X.P. Qiu, J. Power Sources 164 (2007) 555–560.
[14] G.X. Wang, T. Takeguchi, Y. Zhang, E.N. Muhamad, M. Sadakane, S. Ye, W. Ueda, J. Electrochem. Soc. 156 (2009) B862–B869.
[15] S. Jayaraman, T.F. Jaramillo, S.H. Baeck, E.W. McFarland, J. Phys. Chem. B 109 (2005) 22958–22966.
[16] P. Gerard, A. Deneuville, R. Courths, Thin Solid Films 71 (1980) 221–236.
[17] K. Marszalek, Thin Solid Films 175 (1989) 227–233.
[18] B. Gerand, G. Nowogrocki, J. Guenot, M. Figlarz, J. Solid State Chem. 29 (1979) 429–434.
[19] K. Yamanaka, J. Appl. Phys. 26 (1987) 1884–1890.
[20] P.J. Kulesza, L.R. Faulkner, J. Electroanal. Chem. 259 (1989) 81–98.
[21] A.C.C. Tseung, Y. Chen, Catal. Today 38 (1997) 439–443.
[22] F. Maillard, E. Peyrelade, Y. Soldo-Olivier, M. Chatenet, E. Chaînet, R. Faure, Electrochim. Acta 52 (2007) 1958–1967.
[23] Z.H. Zhou, S.L. Wang, W.J. Zhou, G.X. Wang, L.H. Jiang, W.Z. Li, S.Q. Song, J.G. Liu, G.Q. Sun, Q. Xin, Chem. Commun. 3 (2003) 394–395.
[24] C. He, H.R. Kunz, J.M. Fenton, J. Electrochem. Soc. 144 (1997) 970–979.
[25] T. Maiyalagan, B. Viswanathan, J. Power Sources 175 (2008) 789–793.
[26] J. Rajeswari, B. Viswanathan, T.K. Varadarajan, Mater. Chem. Phys. 106 (2007) 168–174.
[27] P.K. Shen, K.Y. Chen, A.C.C. Tseung, J. Electroanal. Chem. 389 (1995) 223–225.
[28] K.W. Park, K.S. Ahn, Y.C. Nah, J.H. Choi, Y.E. Sung, J. Phys. Chem. B 107 (2003) 4352–4355.
[29] X. Zhang, K.Y. Chan, Chem. Mater. 15 (2003) 451–459.
[30] M. Stolze, B. Camin, F. Galbert, U. Reinholz, L.K. Thomas, Thin Solid Films 409 (2002) 254–264.
[31] Z.H. Zhang, X.G. Wang, Z.M. Cui, C.P. Liu, T.H. Lu, W. Xing, J. Power Sources 185 (2008) 941–945.
[32] N.F. Zheng, D.S. Galen, J. Am. Chem. Soc. 128 (2006) 14278–14280.
[33] R. Ganesan, J.S. Lee, J. Power Sources 157 (2006) 217–221.
[34] Z. Hou, B. Yi, H. Yu, Z. Lin, H. Zhang, J. Power Sources 123 (2003) 116–125.